SURFACE TEMPERATURE IMPACT ON THE UPSTREAM DISTURBANCE OF TRUNCATED WEDGE IN HYPERSONIC NON-EQUILIBRIUM FLOW

Wilson F. N. Santos
wilson@lcp.inpe.br
Combustion and Propulsion Laboratory
National Institute for Space Research
Cachoeira Paulista, SP 12630-000

This work describes a computational investigation on rarefied hypersonic flow past truncated wedges. The surface temperature effects on the flowfield structure upstream and adjacent to the body surface have been investigated by employing the Direct Simulation Monte Carlo (DSMC) method. A method that properly accounts for the important aspects of non-equilibrium flow. Aspects that arise near the leading-edge nose and that are especially important at high Mach number flow. The results presented highlight the sensitivity of the primary properties to changes not only on the wall temperature but also on the frontal-face thickness of the leading edges. Some significant differences between sharp and blunt leading edges were noted on the flowfield structure. It was found that the wall temperature variations have different influence on velocity, density, pressure and temperature along the stagnation streamline ahead of the leading edges as well as on the profiles adjacent to the body surface. Interesting features observed in the properties profiles showed that small leading edge thickness, compared to the freestream mean free path, still has important effects on high Mach number leading edge flows.

Keywords: *DSMC, Hypersonic flow, Rarefied flow, Wedge, Wall Temperature.*

1. INTRODUCTION

The resurgence of hypersonic research has increased because of the interest to develop hypersonic vehicle in order to achieve routine, affordable, and reliable access to space. One type of vehicle that is promising for hypersonic flight is the waverider (Nonweiler, 1959). Waverider configurations have received a high degree of interest for their potentially high lift-to-drag (L/D) ratios. A waverider is designed analytically with infinitely sharp leading edges for shock wave attachment. Because the shock wave is attached to the leading edge of the vehicle, the upper and lower surfaces of the vehicle can be designed separately. In addition, the shock wave acts as a barrier in order to prevent spillage of higher-pressure airflow from the lower side of the vehicle to the upper side, resulting in a high-pressure differential and enhanced lift.

Nevertheless, it is extremely difficult to construct a perfectly sharp leading edge. Any manufacturing error results in a significant deviation from the design contour. Moreover, sharp edges are difficult to maintain because they are easily damaged. Additionally, because heat transfer increases inversely with the leading edge radius, high heating is associated with sharp edges. Therefore, for practical hypersonic configurations, leading edges should be blunt for heat transfer, manufacturing and handling concerns. Because blunt leading edge promotes shock wave standoff, practical leading edges will have shock detachment, making leading edge blunting a major concern in the design and prediction of flowfields over waverider configurations.

In this scenario, Santos (2005) has investigated the effect of the leading-edge thickness on the flowfield structure and on the aerodynamic surface quantities over truncated wedges. The emphasis of the work was to provide a critical analysis on maximum allowable geometric bluntness, dictated by heat transfer, handling or manufacturing requirements, resulting on reduced departures from ideal aerodynamic performance of the vehicle. Thus, allowing the blunted leading edge to more closely represents the original sharp leading edge flowfield. The thickness effect was examined for a range of Knudsen number, based on the thickness of the flat face, covering from the transitional flow regime to the free molecular flow one.

Santos (2006) extended the analysis presented by Santos (2005) on truncated wedges by performing a parametric study on these shapes with emphasis placed on the compressibility effects. The primary goal was to assess the sensitivity of the shock wave standoff distance, stagnation point heating and total drag to changes in the freestream Mach number.

Santos (2007) extended further the previous analysis on truncated wedges by examining the impact of the angle of attack on the aerodynamic surface quantities acting on the truncated wedges under hypersonic transition flow conditions. Of particular interest in the analysis was the aerodynamic performance of the leading edges since blunt leading edges at incidence allow leakage of the high-pressure lower surface flow into the upper surface region, causing a reduction in the lift as well as on the L/D ratio. The analysis verified that even the smaller leading edge bluntness resulted in significantly reduction on the L/D ratio.

In an effort to obtain further insight into the nature of the flowfield structure of truncated wedges under hypersonic transitional flow conditions, the present account will examine the impact of the surface temperature on the flowfield properties. The flowfield properties upstream of the leading edge of a body are affected by molecules reflected from the edge region. The importance of the effect is in part conditioned by the edge geometry as well as by the surface conditions, since the molecules are reflected from the body surface with greater energies with increasing the wall temperature.

Under hypersonic transitional flow conditions, at very high speeds and high altitudes, the flow about a given aerodynamic configuration may be sufficiently rarefied that the appropriate molecular mean free path becomes too large, compared to a characteristic length

of the vehicle for the use of continuum assumptions but not large enough for the use of the free molecular theory. In such an intermediate or transition rarefied gas regime, the complete investigation of the flowfield structure would require the full formulation of kinetic theory. The governing equation in the transition regime is the Boltzmann equation (Cercignani, 1988). Nevertheless, in order to circumvent the difficult of a direct solution of the Boltzmann equation, the Direct Simulation Monte Carlo (DSMC) method (Bird, 1994) has been the appropriate choice for problems involving flows of rarefied hypersonic aerothermodynamics.

2.   LEADING-EDGE GEOMETRY

The leading-edge geometries are the same as those presented in the previous work (Santos 2005). The truncated wedges are modeled by assuming a sharp leading edge of half angle θ with a circular cylinder of radius R inscribed tangent to this sharp leading edge. The truncated wedges are also tangents to the sharp leading edge and the cylinder at the same common point. It was assumed a leading edge half angle of 10 degrees, a circular cylinder diameter of 10^{-2}m and frontal-face thickness t/λ_∞ of 0.01, 0.1 and 1, where λ_∞ is the freestream mean free path. Figure 1(a) illustrates schematically this construction. Since the wake region behind the truncated wedges is not of interest in this investigation, it was assumed that the truncated wedges are infinitely long but only the length L is considered.
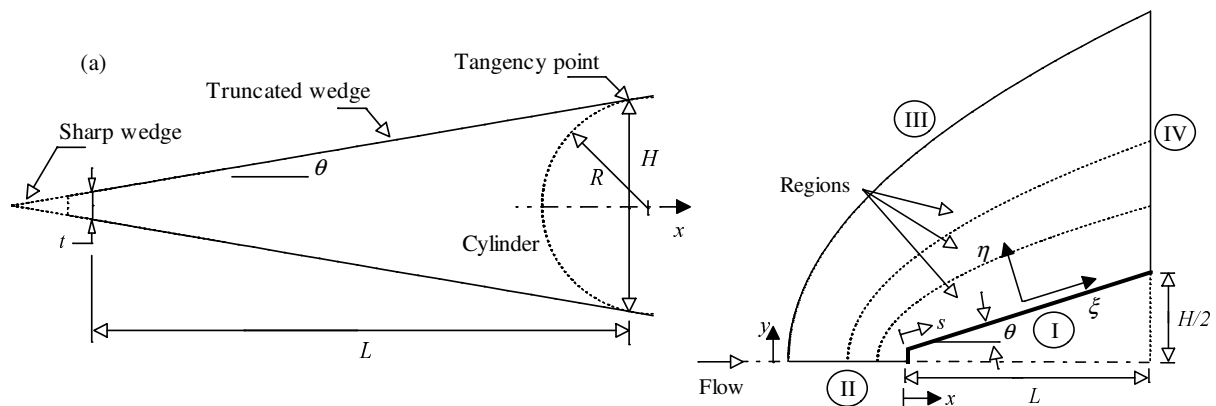

Figure 1: (a) Drawing illustrating the truncated wedge and (b) the computational domain.

3.   COMPUTATIONAL METHOD AND PROCEDURE

The Direct Simulation Monte Carlo (DSMC) method, pioneered by Bird (1994), has become the standard technique for simulating low-density gas dynamics. For these flows, the computational fluid dynamics (CFD) methods that rely on continuum relations to compute the flowfield structure will not provide accurate results in the upper atmosphere, since the assumptions made in developing the differential equations, on which CFD methods are based, break down on rarefied conditions.

The DSMC method simulates real gas flows with various physical processes by means of a huge number of modeling particles, each of which is a typical representative of great number of real gas molecules. DSMC models the flow as being a collection of discrete particles, each one with a position, velocity and internal energy. The state of particles is stored and modified with time as the particles move, collide, and undergo boundary interactions in simulated physical space. The simulation is always calculated as unsteady flow. However, a steady flow solution is obtained as the large time state of the simulation. Therefore, the DSMC method is basically an explicit time-marching algorithm.

Collisions in the present DSMC code are modeled by using the variable hard sphere (VHS) molecular model (Bird, 1981) and the no time counter (NTC) collision sampling technique (Bird, 1989). Repartition energy among internal and translational modes is controlled by the Borgnakke-Larsen statistical model (Borgnakke and Larsen, 1975). Simulations are performed using a non-reacting gas model for a constant freestream gas composition consisting of 76.3% of N_2 and 23.7% of O_2. Energy exchanges between the translational and internal modes, rotational and vibrational, are considered. Relaxation collision numbers of 5 and 50 were used for the calculations of rotation and vibration, respectively.

In the DSMC method, the physical space is divided into an arbitrary number of regions, which are subdivided into a certain number of computational cells, and each cell is also divided into subcells. The physical space network is used to facilitate the choice of molecules for collisions and for the sampling of the macroscopic flow properties such as temperature, pressure, density, etc. In the DSMC algorithm, the linear dimensions of the cells should be small in comparison with the scale length of the macroscopic flow gradients normal to streamwise directions, which means that the cell dimensions should be of the order of or smaller than the local mean free path (Alexander et al., 1998 and 2000). The time step is set such that a typical molecule moves about one third of the cell dimension at each time step. In addition, this time step is much less than the mean collision time (Garcia and Wagner, 2000, and Hadjiconstantinou, 2000), which is defined by the mean time between the successive collisions suffered by any particular molecule.

The computational domain used for the calculation is made large enough so that body disturbances do not reach the upstream and side boundaries, where freestream conditions are specified. A schematic view of the computational domain is depicted in Figure 1(b). Advantage of the flow symmetry is taken into account, and molecular simulation is applied to one-half of a full configuration.

According to Figure 1(b), side I is defined by the body surface. Diffuse reflection with complete thermal accommodation is the condition applied to this side. Side II is a plane of symmetry. In such a boundary, all flow gradients normal to the plane are zero. At the molecular level, this plane is equivalent to a specular reflecting boundary. Side III is the freestream side through which simulated molecules enter and exit. Finally, the flow at the downstream outflow boundary, side IV, is predominantly supersonic and vacuum condition is specified (Guo and Liaw, 2001). At this boundary, simulated molecules can only exit.

Numerical accuracy in DSMC method depends on the grid resolution chosen as well as on the number of particles per computational cell. Both effects were investigated to determine the number of cells and the number of particles required to achieve grid independence solutions. The grid generation scheme used in this study follows that procedure presented by Bird (1994). Along the outer boundary (side III) and the body surface (side I), point distributions are generated in such way that the number of points on each side is the same; ξ-direction in Figure 1(b). Then, the cell structure is defined by joining the corresponding points on each side by straight lines and then dividing each of these lines into segments which are joined to form the system of quadrilateral cells; η-direction in Figure 1(b). The distribution can be controlled by a number of different distribution functions that allow the concentration of points in regions where high flow gradients or small mean free paths are expected.

A grid independence study was made with three different structured meshes in each coordinate direction. The effect of altering the cell size in the ξ-direction was investigated with grids of 50(coarse), 100(standard) and 150(fine) cells, and 60 cells in the η-direction for the bluntest leading edge investigated, $t/\lambda_\infty = 1$ case. In analogous fashion, an examination was made in the η-direction with grids of 30(coarse), 60(standard) and 90(fine) cells, and 100 cells in the ξ-direction for the $t/\lambda_\infty = 1$ case. From the total number of cells in the ξ-direction,

30% are located along the frontal surface and 70% distributed along the afterbody surface. In addition, each grid was made up of non-uniform cell spacing in both directions. The effect (not shown) of changing the cell size in both directions on the heat transfer and pressure coefficients was rather insensitive to the range of cell spacing considered, indicating that the standard grid, 100x60 cells, for the $t/\lambda_\infty = 1$ case, is essentially grid independent. A similar procedure in terms of mesh was performed for the other cases investigated.

In a second stage of the grid independence investigation, a similar examination was made for the number of molecules. The standard grid for the $t/\lambda_\infty = 1$ case, 100x60 cells, corresponds to, on average, a total of 190,000 molecules. Two new cases using the same grid were investigated. These two new cases correspond to 104,000 and 283,000 molecules in the entire computational domain. As the three cases presented approximately the same results (not shown) for the heat transfer, pressure and skin friction coefficients, hence the standard grid with a total of 190,000 molecules is considered enough for the computation of the aerodynamic surface quantities. Again, a similar procedure was performed for the other leading-edge thickness cases investigated.

4. COMPUTATIONAL CONDITIONS

DSMC simulations have been performed for an altitude of 70 km based on the flow conditions given by Santos (2005) and summarized in Table 1, and the gas properties (Bird, 1994) are shown in Table 2. The freestream velocity V_∞ is assumed to be constant at 3.56 km/s. This velocity corresponds to a freestream Mach number M_∞ of 12. The translational and vibrational temperatures in the freestream are in equilibrium at 220 K.

Table 1. Freestream and flow conditions

Temperature T_∞ (K)	Pressure p_∞ (N/m^2)	Density ρ_∞ (kg/m^3)	Number density n_∞ (m^{-3})	Viscosity μ_∞ (Ns/m^2)	Mean free path λ_∞ (m)
220.0	5.582	8.753 x 10^{-5}	1.8209 x 10^{21}	1.455 x 10^{-5}	9.03 x 10^{-4}

Table 2. Gas properties

	Mole fraction X	Molecular mass m (kg)	Molecular diameter d (m)	Viscosity index ω
O_2	0.237	5.312 x 10^{-26}	4.01 x 10^{-10}	0.77
N_2	0.763	4.650 x 10^{-26}	4.11 x 10^{-10}	0.74

The overall Knudsen number Kn is defined as the ratio of the molecular mean free path λ in the freestream gas to a characteristic dimension of the flowfield. In the present study, the characteristic dimension was defined as being the thickness t of the truncated leading edges. For the thicknesses investigated, $t/\lambda_\infty = 0.01$, 0.1 and 1, the overall Knudsen numbers corresponds to $Kn_t = 100$, 10, and 1. Finally, the Reynolds number Re_t covers the range from 0.193 to 19.3, based on conditions in the undisturbed stream with leading edge thickness t as the characteristic length.

In order to simulate the wall temperature effect, the DSMC calculations were performed independently for three distinct numerical values of wall temperature, i.e., T_w of 440 K, 880 K and 1760 K. These values correspond to 2, 4 and 8 times the freestream temperature, respectively. This temperature range is chosen to be representative of the surface temperature near the stagnation point and is assumed to be uniform over the bodies.

5. COMPUTATIONAL RESULTS AND DISCUSSION

The purpose of this section is to discuss and to compare differences in the flowfield properties due to variations on the wall temperature and on the leading-edge thickness. Results will be illustrated by a series of profile plots of velocity, density, pressure and temperature.

5.1 Velocity profile

Normal velocity profiles along the stagnation streamline and their dependence on the body surface temperature are illustrated in Figures 2(a), 2(b) and 2(c) for leading edge thickness t/λ_∞ of 0.01, 0.1 and 1, which correspond to Kn_t of 100, 10 and 1, respectively. In this set of figures, the normal velocity v is normalized by the freestream velocity V_∞, and X is the distance upstream of the leading edges, along the stagnation streamline, normalized by the freestream mean free path λ_∞.

According to these figures, it is seen that the wall temperature as well as the leading-edge thickness influences the flowfield far upstream. This domain of influence increases with increasing either the wall temperature or the leading-edge thickness. The leading-edge thickness effect results from the upstream diffusion of particles that are reflected from the nose of the leading edge. Consequently, blunting the nose of the body (increasing t) leads to significantly larger disturbance upstream of the body. In addition, the wall-temperature effect results from particles reflecting from a hotter surface with greater energies that diffuse further upstream.
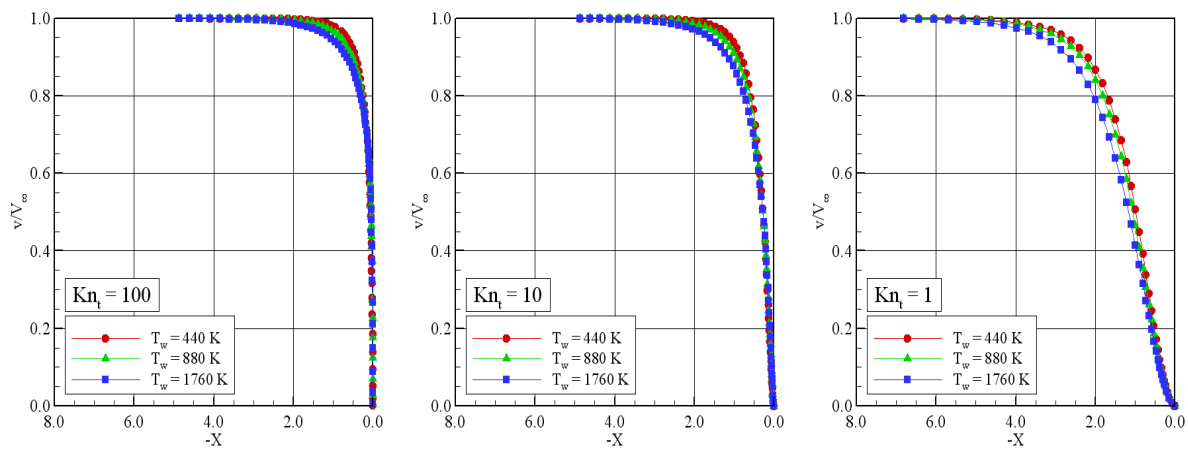

Figure 2: Normal velocity (v/V_∞) profiles along the stagnation streamline as a function of the wall temperature for leading-edge thickness corresponding to Kn_t of (a) 100, (b) 10 and (c) 1.

For comparison purpose, at wall temperature of 440 K, the upstream disturbance for a velocity reduction of 1% ($v/V_\infty = 0.99$) is around $1.27\lambda_\infty$, $1.89\lambda_\infty$ and $3.98\lambda_\infty$ for Kn_t of 100, 10 and 1, respectively. Nevertheless, at wall temperature of 1760 K, the upstream disturbance changes to around $2.32\lambda_\infty$, $2.78\lambda_\infty$ and $4.97\lambda_\infty$ for Kn_t of 100, 10 and 1, respectively.

In an effort to emphasize points of interest, variation of the tangential velocity u in the off-body direction (η-direction) is depicted in Figure 3 as a function of the wall temperature for the $Kn_t = 1$ case. This set of plots presents data at three afterbody stations S of 1, 10 and 20. S stands for the arc length s normalized by the freestream mean free path λ_∞, measured from the shoulder of the leading edges. Of great significance in this set of plots is the slip

velocity. It is seen that the slip velocity increases with increasing the wall temperature. A similar behavior is observed (not shown) for the other two Knudsen number cases investigated, Kn_t of 100 and 10. It should also be noted that the tangential velocity reaches the freestream limit value u_∞ ($u/V_\infty \approx 1$) around $8\lambda_\infty$, $12\lambda_\infty$ and $16\lambda_\infty$ for stations S of 1, 10 and 20, respectively. In contrast, for the sharpest leading edge investigated, $Kn_t = 100$, the tangential velocity reaches (not shown) the limit value around $6\lambda_\infty$, $10\lambda_\infty$ and $14\lambda_\infty$ above the surface for the same respectively stations. It is important to mention that, because of the afterbody slope angle of 10 degrees, u_∞ is given by $V_\infty cos\theta$.
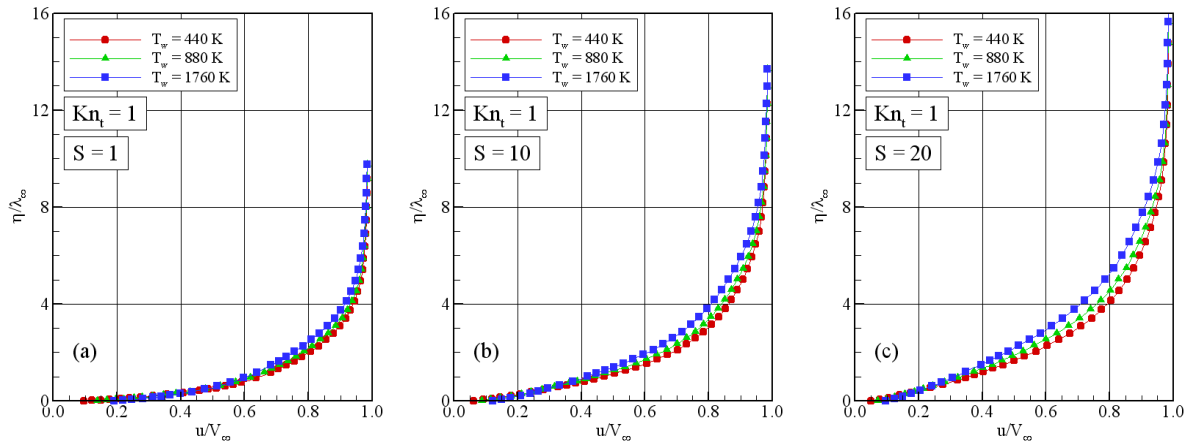

Figure 3: Tangential velocity (u/V_∞) profiles along the afterbody surface as a function of the wall temperature for leading-edge thickness corresponding to Kn_t of 1 at stations that correspond to S of (a) 1, (b) 10 and (c) 20.

5.2 Density profile

Density profiles along the stagnation streamline are plotted as a function of the wall temperature in Figures 4(a), 4(b) and 4(c) for Kn_t of 100, 10 and 1, respectively. In these figures, density ρ is normalized by the freestream density ρ_∞.

The predictions of density for all of the leading-edge thicknesses investigated show no sign of a discrete shock wave. Instead, there is a continuous rise in density from the freestream to the nose of the leading edges, rising to well above the continuum inviscid limit. As a point of reference, the Rankine-Hugoniot relations give a postshock density that corresponds to the ratio $\rho/\rho_\infty = 5.8$ for freestream Mach number of 12. Near the stagnation point, $X \approx 0$, a substantial density increase occurs which is a characteristic of a cold-wall entry flow (Haas and Fallavollita, 1994). In typical entry flow, the body surface temperature is low compared to the stagnation temperature. This leads to a steep density gradient near the body surface. For the present simulation, the ratio of wall temperature to stagnation temperature ranges from 0.07 to 0.27, which correspond to a cold-wall flow.

According to Figures 4(a), 4(b) and 4(c), it can be recognized that density rises gradually as the flow approaches the nose of the leading edges, indicating the diffuse nature of the shock wave, a characteristic of highly rarefied flows. As the wall temperature is increased from 440 K to 1760 K, the particles are reflected from the body surface with greater energies. This leads to greater relative translational velocities and flowfield temperatures. Consequently, energetic reflections from hotter surface reduce the net buildup of particle density near the body surface. By examining the density profiles, two regions are seen; one inner region close to the stagnation point, roughly defined by $X > -0.1$ and $X > -0.3$ for $Kn_t =$

100 and 1, respectively, where variation in the wall temperature affects the density profiles, and an outer region, $X < -0.1$ and $X < -0.3$ for $Kn_t = 100$ and 1, respectively, where virtually no effect is detected due to the wall temperature rise. Furthermore, as the leading edge becomes blunt, i.e., by increasing the frontal-face thickness t, the extent of the flowfield disturbance becomes much larger, as evidenced by the density profiles.

At this point it is worth taking a closer look at density distribution adjacent to the afterbody surface. In doing so, Figure 5 displays selected local density profiles, expressed as a ratio to the freestream density value, for three stations located on the afterbody surface of the leading edge corresponding to the $Kn_t = 1$ case ($t/\lambda_\infty = 1$ case).
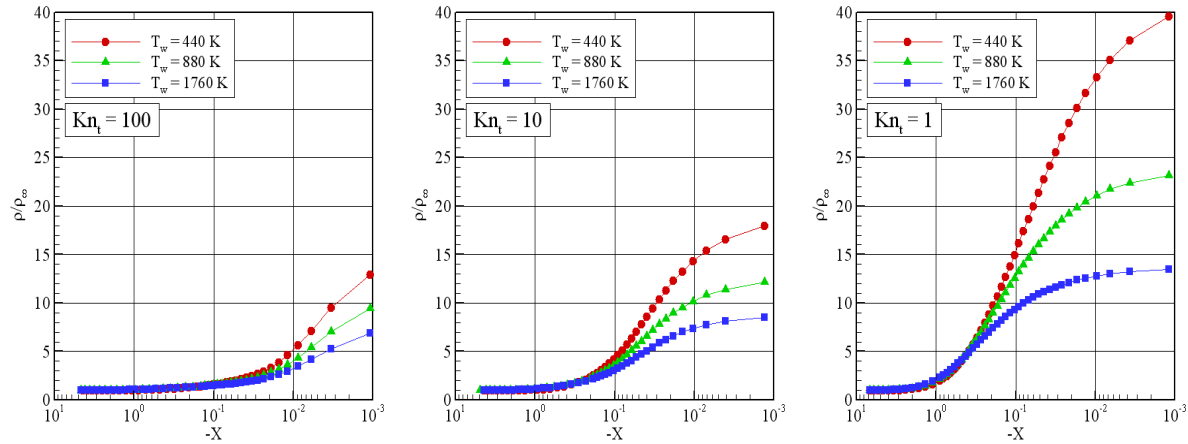

Figure 4: Density (ρ/ρ_∞) ratio profiles along the stagnation streamline as a function of the wall temperature for leading-edge thickness corresponding to Kn_t of (a) 100, (b) 10 and (c) 1.
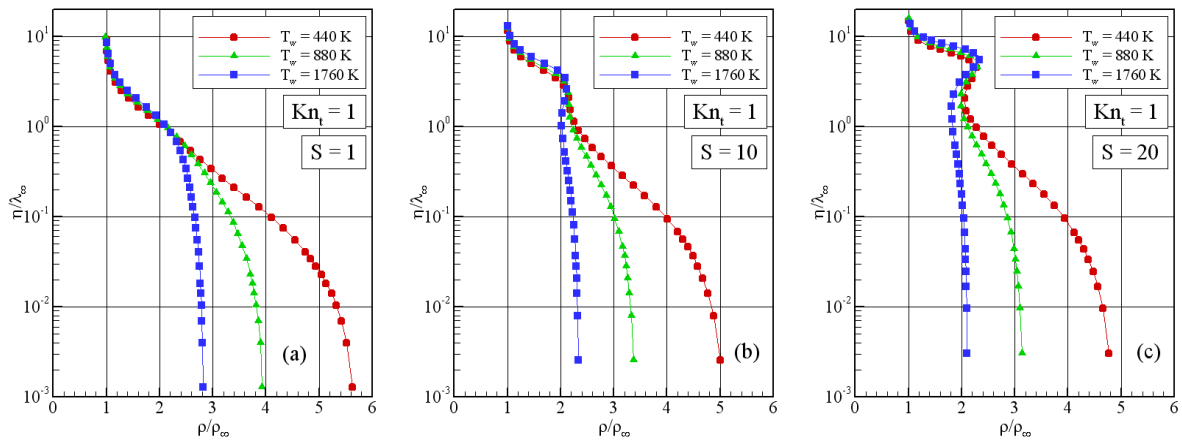

Figure 5: Density (ρ/ρ_∞) ratio profiles along the afterbody surface as a function of the wall temperature for leading-edge thickness corresponding to Kn_t of 1 at stations that correspond to S of (a) 1, (b) 10 and (c) 20.

According to Figures 5(a), 5(b) and 5(c), it is clearly observed that density is affected by the wall temperature rise, as would be expected. For the station corresponding to $S = 1$, Figure 5(a), the density variation is significant for the wall temperature investigated. In this region, close to the shoulder of the leading edge, the compression on the frontal face combined with a relatively cool wall produces a maximum density that is 5.6, 4.0 and 2.8 times the freestream density value for cases with wall temperature of 440 K, 880 K and 1760 K, respectively.

Because of the expansion downstream along the afterbody surface, the density adjacent to the body surface decreases to around 4.8, 3.2 and 2.0 times the freestream density value for wall temperature cases of 440 K, 880 K and 1760 K, respectively, at the station corresponding to $S = 20$, Figure 5(c). This density drop represents a reduction around of 15%.

In what follows, density contours, normalized by the freestream density ρ_∞, are depicted in Figures 6(a), 6(b) and 6(c) for leading edges corresponding to Kn_t of 100, 10 and 1, respectively. In this set of diagrams, X and Y stand for the length x and height y normalized by the freestream mean free path λ_∞. Also, the upper and lower parts represent the leading edge with wall temperature of 440 K and 1760 K, respectively. Referring to this set of diagrams, it is noted that the major changes in density occur in a thin region close to the body surface.
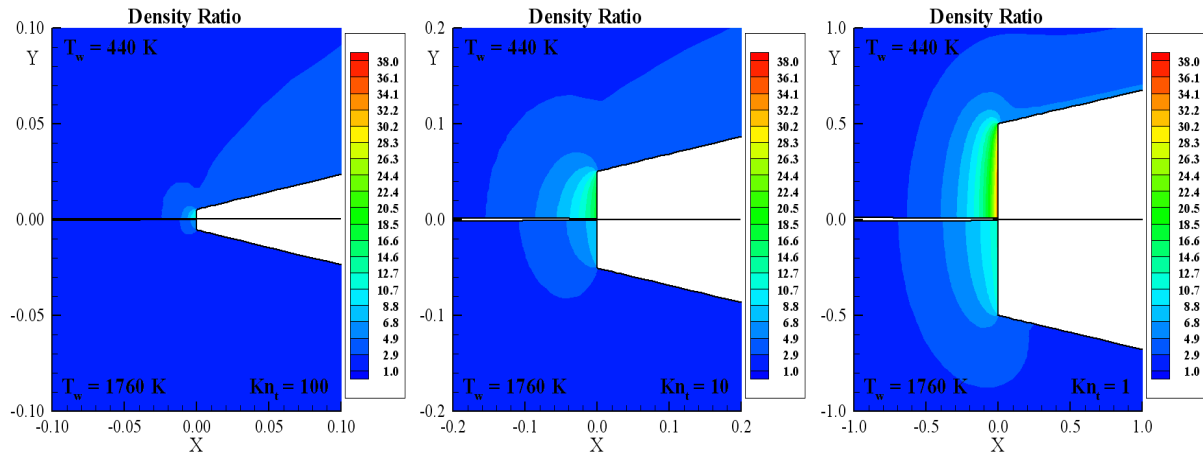

Figure 6: Density (ρ/ρ_∞) ratio contours at the vicinity of the leading-edge nose defined by Kn_t of (a) 100, (b) 10 and (c) 1. Upper and lower parts represent the leading edge with wall temperature of 440K and 1760 K, respectively.

5.3 Pressure profile

The large amount of kinetic energy present in a hypersonic freestream is converted by molecular collisions into high thermal energy surrounding the body and by flow work into increased pressure. In this respect, the stagnation region is a zone of strong compression, where pressure increases from the freestream to the stagnation point due to the shock wave that forms ahead of the leading edges.

Representative pressure profiles along the stagnation streamline are shown as a function of the wall temperature T_w in Figures 7(a), 7(b) and 7(c) for Knudsen number Kn_t of 100, 10 and 1, respectively. In this set of diagrams, the pressure p is normalized by the freestream pressure p_∞. As can be seen in these plots, there is a continuous rise in pressure from the freestream up to the nose of the leading edge. Near the stagnation point, a substantial pressure increase occurs with increasing the leading edge thickness t. It is apparent from these figures that the wall temperature effects are more significant at the vicinity of the stagnation point for sharp and aerodynamic sharp leading edges, i.e., leading edges corresponding to Kn_t of 100 and 10, respectively. In contrast, for the bluntest leading edge, Kn_t of 1, it seems that the general shape of the pressure distribution profiles is preserved when the wall temperature is increased from 440 to 1760 K.

Still referring to Figures 7(a), 7(b) and 7(c), it is clearly noticed that the extent of the upstream flowfield disturbance for pressure is significantly different from that presented by density. The domain of influence for pressure is higher than that for density and lower than that presented for temperature, as will be seen subsequently. Similar to the density, much of

the pressure increase in the shock layer occurs after the translational kinetic temperature has reached its postshock value.

Local pressure, expressed as a ratio to the freestream value, for three stations located on the afterbody surface related to the $Kn_t = 1$ case ($t/\lambda_\infty = 1$ case) is illustrated in Figure 8. It is apparent from these profiles that pressure is not significantly affected by the wall temperature rise, as was mentioned earlier. At the station corresponding to $S = 1$, Figure 8(a), the pressure variation is in excess of one order of magnitude for the wall temperature range investigated. In this region, close to the wedge shoulder, the compression produces a maximum pressure that is around 40 times the freestream pressure value for the wall temperature cases investigated. Due to the expansion downstream along the body surface, the pressure adjacent to the afterbody surface decreases to around 20 times the freestream pressure value for wall temperature cases investigated, at the station corresponding to $S = 20$, as shown in Figure 8(c), a reduction around of 50% in pressure for station S from 1 to 20.
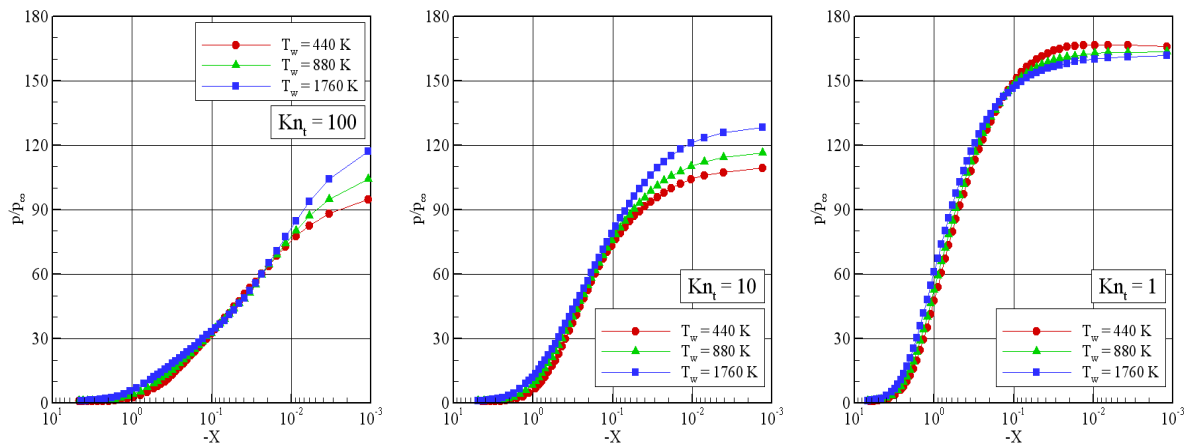

Figure 7: Pressure (p/p_∞) profiles along the stagnation streamline as a function of the wall temperature for leading-edge thickness corresponding to Kn_t of (a) 100, (b) 10 and (c) 1.
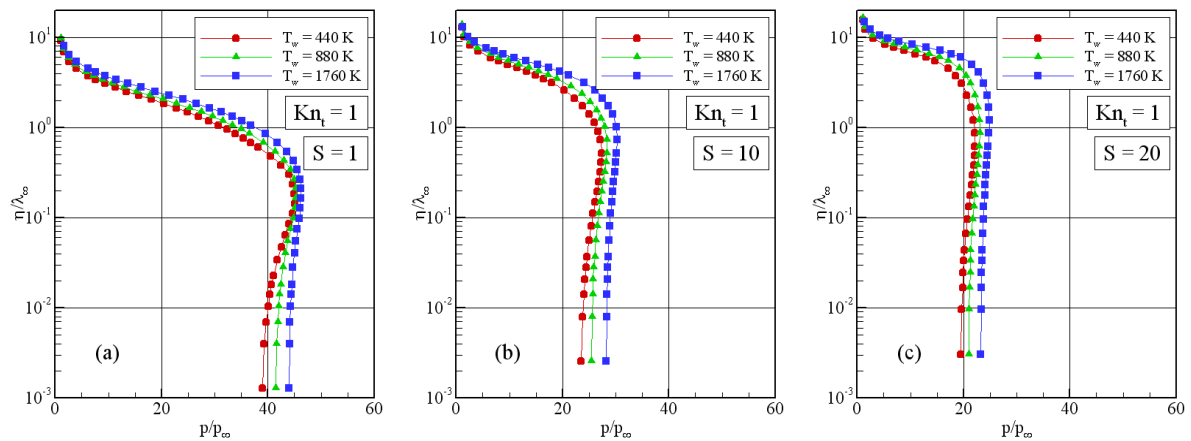

Figure 8: Pressure (p/p_∞) profiles along the afterbody surface as a function of the wall temperature for leading-edge thickness corresponding to Kn_t of 1 at stations that correspond to S of (a) 1, (b) 10 and (c) 20.

In the following, a critical assessment of the flowfield is provided by Figures 9(a), 9(b) and 9(c), which consider a magnification of the pressure ratio, p/p_∞, at the vicinity of the

leading-edge nose for Kn_t of 100, 10 and 1, respectively. This group of figures confirms that the stagnation region is a zone of strong compression. Moreover, the extent of the upstream flowfield disturbance for pressure is significantly different from that presented by density. Also, it is seen that the upstream domain of influence for pressure is higher than that for density and lower than that presented for temperature, as will be subsequently.
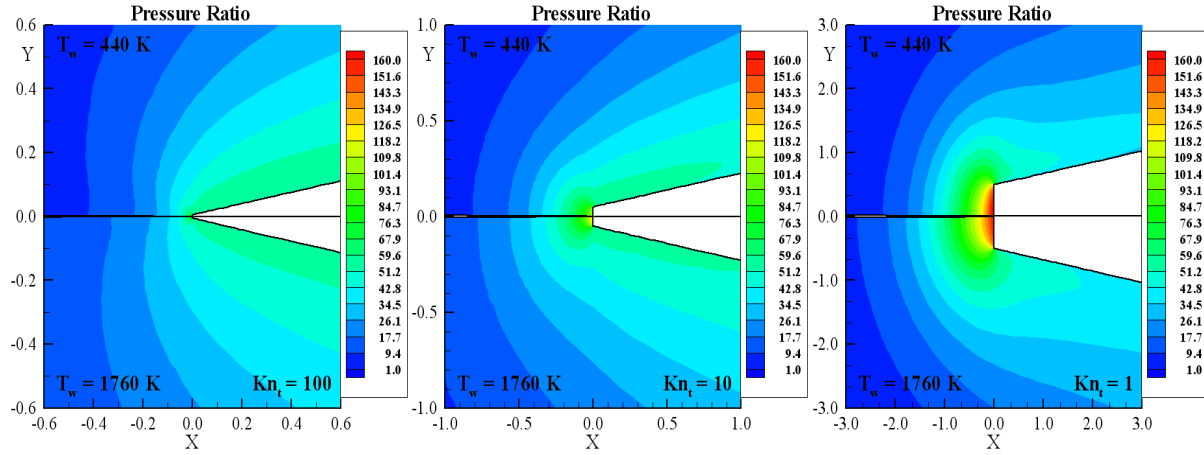

Figure 9: Pressure (p/p_∞) ratio contours at the vicinity of the leading-edge nose defined by Kn_t of (a) 100, (b) 10 and (c) 1. Upper and lower parts represent the leading edge with wall temperature of 440K and 1760 K, respectively.

5.4 Temperature profile

The strong shock wave that forms ahead of a blunt leading edge at hypersonic flow converts part of the kinetic energy of the freestream air molecules into thermal energy. This thermal energy downstream of the shock wave is partitioned into increasing the translational kinetic energy of the air molecules, and into exciting other molecular energy states such as rotation and vibration.

Kinetic temperature profiles along the stagnation streamline are demonstrated in Figures 10(a), 10(b) and 10(c) for thickness Knudsen number Kn_t of 100, 10 and 1, respectively. for wall temperature cases of 440 and 1100 K, respectively. In this set of diagrams, the kinetic temperatures are normalized by the freestream temperature T_∞. In addition, filled and empty symbols stand for the wall temperature T_w of 440 K and 1760 K, respectively. It is apparent from these figures that thermodynamic non-equilibrium occurs throughout the shock layer, as shown by the lack of equilibrium of the translational and internal kinetic temperatures. Thermal non-equilibrium occurs when the temperatures associated with the translational, rotational, and vibrational modes of a polyatomic gas are different. In this scenario, it proves convenient to define the overall kinetic temperature, obtained for a non-equilibrium gas as the weighted mean of the translational and internal temperatures.

The overall kinetic temperature shown in the plots is defined for a non-equilibrium gas (Bird, 1994) as follows,

$$T_{OV} = \frac{\zeta_T T_T + \zeta_R T_R + \zeta_V T_V}{\zeta_T + \zeta_R + \zeta_V} \qquad (1)$$

where ζ is the degree of freedom, and subscripts T, R and V stand for translational, rotational and vibrational modes.

The overall kinetic temperature is equivalent to the thermodynamic temperature only under thermal equilibrium conditions. It should be remarked that the ideal gas equation of state does not apply to this temperature in a non-equilibrium situation.
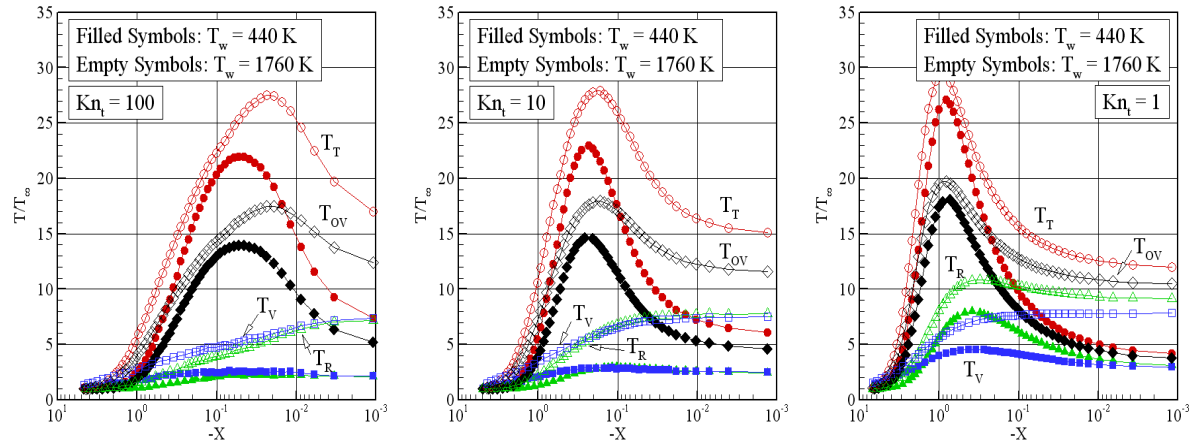

Figure 10: Kinetic temperature (T/T_∞) profiles along the stagnation streamline as a function of the wall temperature for leading-edge thickness corresponding to Kn_t of (a) 100, (b) 10 and (c) 1. Filled and empty symbols stand for wall temperature of 440 K and 1760 K, respectively.

Referring to Figure 10, in the undisturbed freestream far from the body, the translational and internal temperatures have the same value and are equal to the thermodynamic temperature. Approaching the nose of the leading edge, the translational temperature rises to well above the rotational and vibrational temperatures and reaches a maximum value that is a function of the leading-edge thickness as well as of the wall temperature T_w. Since a large number of collisions is needed to excite molecules vibrationally from the ground state to the upper state, the vibrational temperature increases more slowly than rotational temperature. Still further downstream toward the nose of the leading edge, the translational temperature decreases and reaches a value on the frontal face that is above the wall temperature, resulting in a temperature jump as defined in continuum formulation.

The substantial rise in translational kinetic temperature for the leading edges occurred before the density rise (see Figure 4). As a base of comparison, the kinetic translational temperature T_T reaches the maximum value around a distance of one freestream mean free path from the frontal face of the leading edge corresponding to $Kn_t = 1$ and $T_w = 440$ K, while the density ratio ρ/ρ_∞ is around 1.8 at the same station. The translational kinetic temperature rise for blunt leading edges results from the essentially bimodal velocity distribution (Liepmann et al., 1964): the molecular sample consisting of mostly undisturbed freestream molecules with the molecules that have been affected by the shock and reflected from the body. In this connection, the translational kinetic temperature rise is a consequence of the large velocity separation between these two classes of molecules.

In the following, it becomes instructive to illustrate the effect on the overall kinetic temperature along the leading-edge surface due to the changes on the wall temperature T_w. In this respect, the overall kinetic temperature variations is taken normal to the body surface at afterbody stations corresponding to S of 1, 10 and 20 measured from the shoulder of the leading edges.

Figure 11 depict profiles of overall kinetic temperature ratio for Kn_t of 1 at the considered positions along the afterbody surface. In this set of figures, the overall kinetic temperature T_{OV} is normalized by the freestream temperature T_∞. According to these plots, it is observed that the downstream evolution of the flow displays a smearing tendency of the shock wave due to

the displacement of the maximum value for the overall kinetic temperature. Also, it may be recognized from Figure 11 that the overall kinetic temperature reaches a value close to the afterbody surface that is above the wall temperature, resulting in a significant temperature jump. The temperature jump behavior observed is similar to the slip velocity one (see Figure 3) in that both temperature jump and slip velocity increase on the body surface with the wall temperature rise.

In order to bring out important features of the wall temperature effects, particular attention is paid to the overall kinetic temperature at the vicinity of the frontal face of the leading edges. In this context, overall kinetic temperature contours, normalized by the freeestream temperature T_∞, are plotted in Figures 12(a), 12(b) and 12(c) for leading edges corresponding to Kn_t of 100, 10 and 1, respectively. Again, in these figures, X and Y stand for the length x and height y normalized by the freestream mean free path λ_∞. Also, the upper and lower parts represent the leading edge with wall temperature of 440 K and 1760 K, respectively.
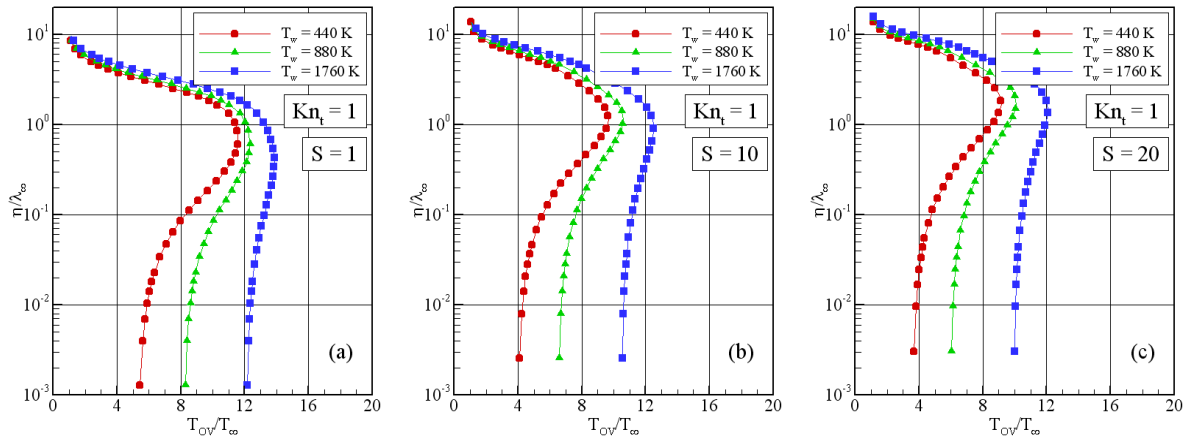

Figure 11: Overall temperature (T_{OV}/T_∞) profiles along the afterbody surface as a function of the wall temperature for Kn_t of 1 at afterbody stations that correspond to S of (a) 1, (b) 10 and (c) 20.

Figure 12: Overall temperature (T_{OV}/T_∞) profiles along the afterbody surface as a function of the wall temperature for Kn_t of 1 at afterbody stations that correspond to S of (a) 1, (b) 10 and (c) 20.
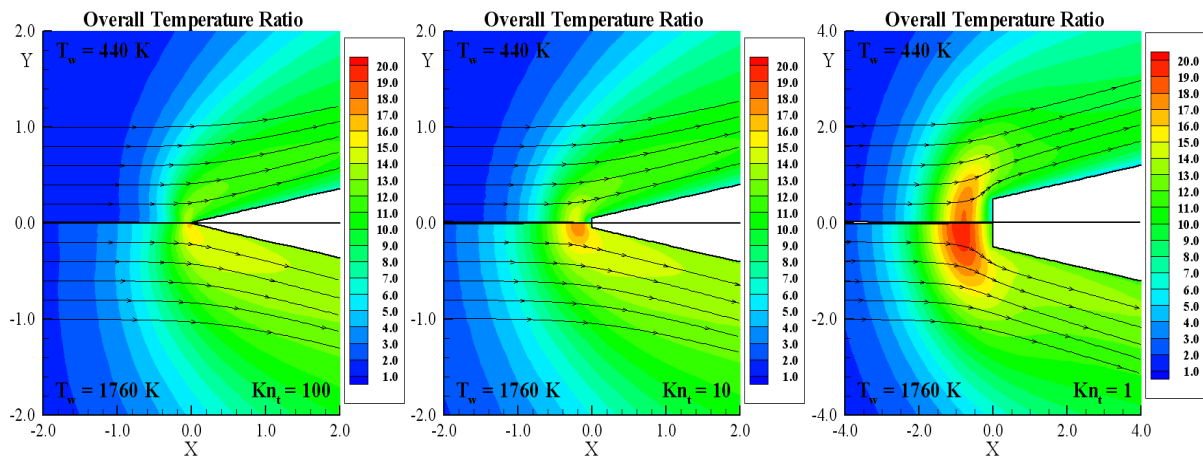
Substantial differences in the overall kinetic temperature are observed not only as the thickness Knudesn number Kn_t changes from 100 to 1 but also as the wall temperature increases from 440 K to 1760 K. For instance, the overall kinetic temperature core is located roughly on the nose of the leading edge for the $Kn_t = 100$ case. Nevertheless, it is about one freestream mean free path ahead of the stagnation point for the $Kn_t = 1$ case, showing that the upstream disturbance becomes more pronounced as the leading edge becomes blunter. Of particular interest is the upstream disturbance caused by the temperature rise. It is thus firmly established that the upstream disturbance increases by increasing the wall temperature.

6. CONCLUDING REMARKS

Computations of a rarefied hypersonic flow on sharp and blunt leading edges have been performed by using the Direct Simulation Monte Carlo method. The calculations provided information concerning the nature of the flowfield structure about the primary properties at the vicinity of the frontal face and immediately adjacent to the afterbody surface for a family of truncated wedges.

Effects of body surface temperature on the velocity, density, pressure, and temperature for a wide range of parameters were investigated. The wall temperature varied from 440 K to 1760 K, set to be from 2 to 8 times the freestream temperature. In addition to that, the leading-edge thickness ranged from 0.01 to 1 of the freestream mean free path, corresponding thickness Knudsen numbers from 100 to 1. Cases considered in this study covered the hypersonic flow from the transitional flow regime to the free molecular flow regime.

It was found that changes on the frontal-face thickness as well as on the wall temperature disturbed the flowfield far upstream, as compared to the freestream mean free path, and the domain of influence increased by increasing the nose thickness, as the leading edge becomes blunt, or by increasing the wall temperature. Moreover, the extent of the upstream flowfield disturbance is significantly different for each one of the flow properties. The domain of influence for temperature is larger than that observed for pressure and density. Since the extent of the flowfield disturbance is significantly different for each one of the leading edge shapes, this will have important implications in problems that take into account for the gas-phase chemistry and for the gas-surface catalytic activity.

It is important to emphasize that this investigation has taken into account for a representative number of effects. Nevertheless, a number of improvements to a realistic leading edge design is still desirable. The DSMC method has been used to assess the flowfield structure on truncated wedges by considering constant wall temperature. In a realistic design, temperature not only changes along the body surface but also inside the leading edge. In this scenario, a more detailed analysis that includes the conjugate heat transfer problem seems to be challenge.

7. REFERENCES

Alexander, F. J., Garcia, A. L., and, Alder, B. J., 1998, Cell size dependence of transport coefficient in stochastic particle algorithms. *Physics of Fluids*, vol. 10, n. 6, pp. 1540-1542.

Alexander, F. J., Garcia, A. L., and, Alder, B. J., 2000, Erratum: cell size dependence of transport coefficient is stochastic particle algorithms. *Physics of Fluids*, vol. 12, n. 3, pp. 731-731.

Bird, G. A., 1981, Monte Carlo simulation in an engineering context. In Fisher, S. S., ed, *Progress in Astronautics and Aeronautics: Rarefied gas Dynamics*, vol. 74, part I, AIAA New York, pp. 239-255.

Bird, G. A., 1989, Perception of numerical method in rarefied gasdynamics. In Muntz, E. P., Weaver, D. P. & Capbell, D. H., eds, *Rarefied gas Dynamics: Theoretical and Computational Techniques*, vol. 118, AIAA, New York, pp. 374-395.

Bird, G. A., 1994, *Molecular Gas Dynamics and the Direct Simulation of Gas Flows*, Oxford University Press, Oxford, England, UK.

Borgnakke, C. and Larsen, P. S., 1975, Statistical collision model for Monte Carlo simulation of polyatomic gas mixture. *Journal of computational Physics*, vol. 18, n. 4, pp. 405-420.

Cercignani, C., 1988, *The Boltzmann Equation and Its Applications*, Springer-Verlag, New York, NY.

Garcia, A. L., and, Wagner, W., 2000, Time step truncation error in direct simulation Monte Carlo. *Physics of Fluids*, vol. 12, n. 10, pp. 2621-2633.

Haas, B. L. and Fallavollita, M. A., 1994, Flow resolution and domain influence in rarefied hypersonic blunt-body flows, *Journal of Thermophysics and Heat Transfer*, vol. 8, n. 4, pp. 751-757.

Hadjiconstantinou, N. G., 2000, Analysis of discretization in the direct simulation Monte Carlo. *Physics of Fluids*, vol. 12, n. 10, pp. 2634-2638.

Liepmann, H. W., Narasimha, R. and Chahine, M., 1964, Theoretical and experimental aspects of the shock structure problem. In H. Gortler, ed., *Proceedings of the 11th International Congress of Applied Mechanics*, Munich, Germany, pp. 973-979.

Nonweiler, T. R. F., 1959, Aerodynamic problems of manned space vehicles. *Journal of the Royal Aeronautical Society*, vol. 63, Sept, pp. 521-528.

Santos, W. F. N., 2005, Flat-faced leading-edge effects in low-density hypersonic wedge flow. *Journal of Spacecraft and Rockets*, vol. 42, n. 1, pp. 22-29.

Santos, W. F. N., 2006, Effects of compressibility on aerodynamic surface quantities over low-density hypersonic wedge flow. *Journal of the Society of Mechanical Sciences and Engineering*, vol. 28, n. 3, pp. 311-321.

Santos, W. F. N., 2007, Leading edge thickness impact on drag and lift in hypersonic wedge flow. *Proceedings of the 45th AIAA Aerospace Sciences Meeting and Exhibit*, AIAA Paper 2007-0615, Reno, NV.